GLD360 Performance Relative to TRMM LIS

SCOTT D. RUDLOSKY

National Oceanic and Atmospheric Administration/National Environmental Satellite, Data, and Information Service/Center for Satellite Applications and Research, and Cooperative Institute for Climate and Satellites, Earth System Science Interdisciplinary Center, and Department of Atmospheric and Oceanic Science, University of Maryland, College Park, College Park, Maryland

MICHAEL J. PETERSON

Cooperative Institute for Climate and Satellites, Earth System Science Interdisciplinary Center, University of Maryland, College Park, College Park, Maryland

DOUGLAS T. KAHN

Department of Atmospheric and Oceanic Science, University of Maryland, College Park, College Park, Maryland

ABSTRACT

This study evaluates the performance of the operational and reprocessed Global Lightning Dataset 360 (GLD360) data relative to the Tropical Rainfall Measuring Mission (TRMM) Lightning Imaging Sensor (LIS) during 2012–14. The analysis compares ground- and space-based lightning observations to better characterize the pre- and postupgrade GLD360. The reprocessed, postupgrade data increase the fraction of LIS flashes detected by the GLD360 [i.e., relative detection efficiency (DE)]. The relative DE improves during each year in every region, and year-over-year improvement appears in both datasets. The reprocessed relative DE exceeds 40% throughout large portions of the study domain with relative maxima over the western Atlantic, eastern Pacific, and the Gulf of Mexico. The upgrade results in shorter distances between matched LIS and GLD360 locations, indicating improved location accuracy. On average, the matched LIS flashes last longer (18.6 ms) and are larger (379.3 km^2) than the unmatched LIS flashes (6.1 ms, 251.0 km^2). For each LIS characteristic examined, the greater the value, the more likely the GLD360 detects the flash. Of the matched LIS flashes, 44.3% have multiple GLD360 strokes, and the mean LIS characteristics increase with increasing stroke count. LIS flashes with four-plus related GLD360 strokes are longest (61.1 ms) and largest (492.7 km^2). Of the multistroke flashes, 57.3% contain subsequent strokes that are stronger than the initial stroke. The vast majority of multistroke flashes with a first stroke estimated with a peak current of <10 kA have stronger subsequent strokes, suggesting that the GLD360 sometimes detects the initial cloud pulses associated with ground flashes.

1. Introduction

Various ground- and space-based instruments observe the radio and optical emissions produced by lightning. The resulting lightning data have various operational applications on many different spatial and temporal scales (e.g., severe storm warning operations). Much of the recent lightning research in the United States has been in preparation for the Geostationary Operational Environmental Satellite R Series (GOES-R) Geostationary Lightning Mapper (GLM; Goodman et al. 2013). No present sensors match the GLM performance throughout the GLM domain, so data from multiple lightning detection networks have been used for GLM preparation. National Weather Service (NWS) forecasters are most familiar with data from ground-based lightning detection networks because they have had access to the National Lightning Detection Network (NLDN) data over the contiguous United States (CONUS)

---

since the early 1990s. Outside CONUS (OCONUS) forecasters have relied on data from the World Wide Lightning Location Network (WWLLN; Rodger et al. 2004), the Earth Networks Total Lightning Network (ENTLN; Liu and Heckman 2012), and the Vaisala Global Lightning Dataset 360 (GLD360; Said et al. 2010). Recent research and training efforts have sought to leverage this existing knowledge to help prepare NWS forecasters for the GLM era.

The Tropical Rainfall Measuring Mission (TRMM) Lightning Imaging Sensor (LIS) provides optical lightning observations and is more similar to the GLM than the ground-based networks. However, the low-Earth-orbiting TRMM LIS observes lightning for only ~90 s as it passes overhead, whereas the GLM in geostationary orbit provides continuous observations in space and time throughout the GOES field of view. Rudlosky and Shea (2013) evaluated the performance of the WWLLN relative to TRMM LIS and Rudlosky (2015) intercompared the TRMM LIS with the ENTLN. These studies revealed interesting relationships between the ground- and space-based lightning observations and helped motivate the present study. This study evaluates the performance of the GLD360 relative to the TRMM LIS during 2012–14. A recent upgrade to the GLD360 motivated analysis of the operational GLD360 dataset alongside data that have been reprocessed using the upgraded algorithms (Said and Murphy 2016). This analysis aims to characterize better the pre- and postupgrade GLD360 performance, to identify relationships between the ground- and space-based observations, and to provide forecasters with information to help leverage their GLD360 experience to better apply the GLM observations. This manuscript describes the data and methods in sections 2a and 2b, respectively, followed by the results (section 3) and discussion (section 4).

2. Data and methods

a. Data

The GLD360, owned and operated by Vaisala Inc., detects some fraction of lightning globally. The ground-based GLD360 sensors (locations not disclosed) measure very low-frequency (VLF; ~500 Hz to ~50 kHz) atmospheric radio signals (sferics) generated by lightning (Said and Murphy 2016). The GLD360 reports lightning strokes, which in this radio frequency range are dominated by cloud-to-ground (CG) return strokes. The GLD360 also detects other pulselike discharges that produce large radiation fields that are generally associated with preliminary breakdown, leader pulses near ground, and K changes that

occur in cloud during flashes (K, Cummins 2016, personal communication). The network is unique among long-range lightning detection networks because it uses both time-of-arrival and magnetic direction-finding technology (Said and Murphy 2016). The GLD360 uses a waveform recognition and matching algorithm and applies a propagation correction to recover more consistent arrival times across a wide range of distances and propagation conditions (Said and Murphy 2016). An attenuation model also is applied to the amplitude of the waveform to recover an estimated peak current I_p (Said and Murphy 2016).

Said et al. (2010, 2013) detailed the GLD360 detection methodology, which the remainder of this paragraph paraphrases. The waveform matching algorithm begins by cross correlating the measured sferic with a locally stored waveform bank. The waveform bank is composed of sferic waveforms from negative CG strokes indexed at distances ranging from 100 to 6000 km. There is a separate waveform bank for daytime and nighttime propagation conditions. Each detected sferic is cross correlated with the appropriate waveform bank using both the sferic and its negative (i.e., inverse). The peak cross correlation of each polarity determines an estimated distance for that polarity. Once an initial location fix is determined at the central processor, the true propagation distance to each sensor is compared with the estimated propagation distances for each polarity. The polarity that results in the smallest estimated propagation distance error gives the estimated polarity from the respective sensor. The overall polarity for the discharge is determined from a weighted sum of the polarity estimates from each contributing sensor. The resulting dataset provides a record of all lightning discharges observed by at least three GLD360 sensors (Said et al. 2010).

Previous studies have evaluated the GLD360 performance relative to other ground-based lightning observations. Said et al. (2013) compared GLD360 observations to the NLDN data for the period of 21 July 2011–21 July 2012. They found a 57% ground flash detection efficiency (DE), a 2.5-km median location error, a 21% mean peak current error, and 96% correctly matched polarity. Mallick et al. (2014) characterized the GLD360 performance using rocket-and-wire-triggered lightning data acquired at Camp Blanding, Florida, during 2011–13. They found detection efficiencies of 67% for flashes, 37% for strokes, and 4.8% for superimposed pulses. The median location error was 2.0 km, and the median absolute current estimation error was 27% (Mallick et al. 2014).

Several European studies also have evaluated the GLD360 performance. Pohjola and Mäkelä (2013)

compared GLD360 data from May to September 2011 with data from the European Cooperation for Lightning Detection (EUCLID) network. They showed that the GLD360 relative detection efficiency varies from 36% to 170% over Europe, that the median relative location accuracy of GLD360 in Austria in July is 2.8 km, and that the correlation coefficient r between EUCLID and GLD360 I_p is 0.72. Poelman et al. (2013) evaluated the performance of three lightning detection networks relative to 57 negative CG flashes, with 210 total strokes in Belgium during August 2011. They found that the first stroke has a greater chance of being detected than the subsequent strokes for all three networks. They linked this to the fact that the first strokes exhibited greater I_p than the subsequent strokes in these negative CG flashes. For the GLD360, Poelman et al. (2013) found a 70% stroke DE, 79% first-stroke DE, 66% subsequent-stroke DE, 96% flash DE, 6.1-km median location accuracy (LA), -23.4-kA median first-stroke I_p, and -17.4-kA median subsequent stroke I_p.

The GLD360 underwent an upgrade on 18 August 2015 that involved algorithm changes to the central processor (Said and Murphy 2016). Vaisala has since reprocessed the GLD360 archive back to 1 January 2012 using the upgraded algorithms (referred to as reprocessed data in this study). Said and Murphy (2016) noted that the primary changes include a more refined propagation model, improved sensor correlation heuristics, and a more robust backend infrastructure. Their study evaluated the operational and reprocessed datasets relative to the NLDN. During 2014, they showed that the operational (reprocessed) GLD360 dataset reported 822 (1480) million strokes. In both the operational and reprocessed datasets, the relative flash DE decreases with decreasing peak current magnitude. However, the flash DE of the reprocessed dataset is higher compared to the operational dataset for every peak current range. Integrated over all peak current bins, the total CG flash DE increased from 59% to 81%. The reprocessed (operational) dataset detected 44% (21%) of the NLDN reported cloud pulses. The postupgrade performance best reflects the current real-time GLD360 performance.

The relative DE of the reprocessed dataset exhibits significantly less diurnal variation than the operational dataset (Said and Murphy 2016). The overall NLDN-relative flash DE for the reprocessed dataset holds near 85% for the nighttime and early/late daytime hours. During the peak activity in the late local afternoon hours, the relative CG flash DE dips to 76%. This dip is correlated with the increase in total flash counts, rather than with a change in day/night ionospheric propagation profiles. The dip is likely caused by count saturation

effects at the sensor and central processor (i.e., too many signals to process) and not due to the diurnal dependence of propagation losses in the Earth–ionosphere waveguide. In contrast, the relative DE of the operational dataset varies between 50% and 70%, and is at a minimum during local midnight. Adjustments to the waveform identification scheme, improvements to the propagation correction parameters, and other modifications to the location algorithm improved the median location accuracy from 2.4 to 1.8 km, and the 90th percentile location error from 12.9 to 6.4 km. All GLD360 data since 18 August 2015 are produced using the new algorithms.

The TRMM LIS is an optical transient detector that identifies lightning flashes by detecting the discrete optical pulses associated with changes in cloud brightness at each pixel (Christian et al. 1992). It was launched into low-Earth orbit (350 km) in November 1997, providing coverage between 38°N and 38°S (Christian et al. 1999). The LIS has a sampling rate slightly greater than 500 frames per second with a spatial resolution of between 3 km at nadir and 6 km at the limbs (Christian et al. 1999). Its orbit was boosted to ~400 km in 2001 to increase mission lifetime, with no impact on DE (Cecil et al. 2014). The TRMM LIS reports the time, location, and radiant energy of total lightning events (Christian et al. 1999). Since both intracloud (IC) and CG flashes emit optical pulses, both types are readily observed from above (Christian et al. 1992). Individual lightning events (illuminated pixels) are combined into groups, flashes, and areas using optical pulse-to-flash and flash-to-cell clustering algorithms (Boccippio et al. 2002). Adjacent (i.e., with a side or corner touching) simultaneous events are combined to form groups. Groups are further combined into flashes using a weighted Euclidean distance method with spatial and temporal criteria of 5.5 km and 330 ms (Mach et al. 2007). LIS observations have been cross calibrated with ground-based lightning detection networks (e.g., Thomas et al. 2000; Ushio et al. 2002) and used to create global lightning climatologies (e.g., Christian et al. 1999; Cecil et al. 2014, Albrecht et al. 2016).

The LIS detection efficiency is directly related to the relative brightness of the lightning events, which varies based on the time of day and flash characteristics (e.g., IC/CG, current, and altitude). The LIS observes ~90% of lightning flashes at night and ~70% at local noon (Boccippio et al. 2002; Cecil et al. 2014). The TRMM has a low-altitude, low-inclination orbit that precesses through the local diurnal cycle (Simpson et al. 1988), reducing the impact of diurnal DE variability on annual lightning climatologies. The LIS samples only while overhead, approximately 0.1% of the time in the tropics, but this is sufficient to produce accurate annual climatologies (Christian et al. 1999, 2003). Although the LIS

observes some flashes more efficiently than others, our analysis assumes that the LIS observes all lightning within its field of view. The intensity of LIS flashes (i.e., the amount of charge transferred) can be inferred from their radiance (brightness), duration, and area (Peterson and Liu 2013; Peterson et al. 2016). LIS flash locations represent a radiance-weighted centroid based on all of the LIS events and groups included in each flash. Zhang et al. (2016) reported a roughly 5-km-distance offset in the latitudinal location of the LIS group-level data relative to spatially and temporally correlated NLDN discharges. This inherent distance offset is accounted for by our matching methods, and contributes to the location differences between LIS flashes and GLD360 strokes described herein. The LIS data are missing for 31 days during 2014, with 9, 15, and 7 days missing in August, September, and October, respectively.

The lightning detection network performance varies based on differing environmental conditions. For example, the GLM detects a larger fraction of lightning during the nighttime than daytime due to the greater brightness contrast between the lightning and the background. The GLD360 also performs better at night, but the daytime dip is most likely related to a signal saturation effect due to the increase in total flash counts, rather than with a change in day/night ionospheric propagation profiles (Said and Murphy 2016). Our analysis does not address the diurnal variability inherent in both the LIS and GLD360 observations. The present study does not investigate the LIS performance (i.e., the fraction of GLD360 flashes observed by the LIS) despite the important insights that are gained by doing so. Other studies have investigated LIS performance (e.g., Boccippio et al. 2002; Mach et al. 2007; Bitzer et al. 2016), and similar studies will be required to characterize the GLM. The present study also does not directly measure how well the GLD360 observes the propagation and spatial extent of flashes, only the efficiency at which the GLD360 detects LIS flashes (i.e., not LIS groups or events). The results presented herein provide a baseline for more detailed future analyses of regional, seasonal, and diurnal GLD360 performance variability.

b. Methods

Previous comparisons of ground- and satellite-based lightning observations have used both flash density comparisons (e.g., Boccippio et al. 2002) and more complex flash-by-flash comparisons (e.g., Thomas et al. 2000; Ushio et al. 2002; Rudlosky and Shea 2013; Rudlosky 2015). This study matches individual LIS flashes with GLD360 strokes to examine the spatial and temporal distributions of GLD360 performance relative to the LIS. Direct flash-to-stroke comparisons reveal the

location differences (offsets) between matched flashes, the number of GLD360 strokes associated with each matched LIS flash, and the LIS characteristics (e.g., duration and area) of matched and unmatched flashes. Our analysis assumes that the LIS observes all lightning flashes in its field of view, and no attempt was made to correct for diurnal DE variability. Unlike the limited LIS field of view, the GLD360 continuously detects some fraction of lightning across the globe. Although the GLD360 is a global dataset, the present study domain includes only the Western Hemisphere between 25°S and 38.5°N. The eastern, western, and southern boundaries are the extent of the GLD360 data made available for this study, and the northern boundary represents the northernmost extent of the TRMM LIS observations.

The matching methods used in this study are identical to those used by Rudlosky and Shea (2013) and Rudlosky (2015). LIS flashes comprise multiple LIS groups whose times and locations are used to define the spatial and temporal extents of LIS flashes. For LIS flashes to be considered a match, a GLD360 stroke must occur within 25 km of any group in an LIS flash (i.e., farthest groups north, south, east, and west). The rectangle swept out by these spatial bounds is larger than the LIS footprint to account for uncertainties in the location accuracy of both networks. A GLD360 stroke must occur within 330 ms before, during, or 330 ms after an LIS flash to be consider a match. Although LIS groups are used to define the beginning, end, and spatial extents of each LIS flash, we report only the fraction of LIS flashes detected by the GLD360 (i.e., not the fraction of LIS groups or LIS events). Multiple GLD360 strokes often occur during individual matched LIS flashes, and we use the time and location of the first GLD360 stroke rather than the nearest in time or space for the statistics. The relative flash DE is the fraction of all LIS flashes in a region that are detected (matched) by the GLD360. Maps of relative flash DE are computed by dividing the sum of the "matched" LIS flashes (i.e., those seen by the GLD360) by the sum of "all" LIS flashes within $2° \times 2°$ grid cells. The spatial plots are complemented by tables displaying the reprocessed GLD360 relative DE in individual regions (i.e., United States, land, oceans, North America, South America, Central America, Caribbean Islands, and western Africa) as well as all countries in the study domain with at least 1000 LIS flashes.

3. Results

Counts of LIS flashes and GLD360 strokes depict similar spatial patterns (Fig. 1) despite large differences
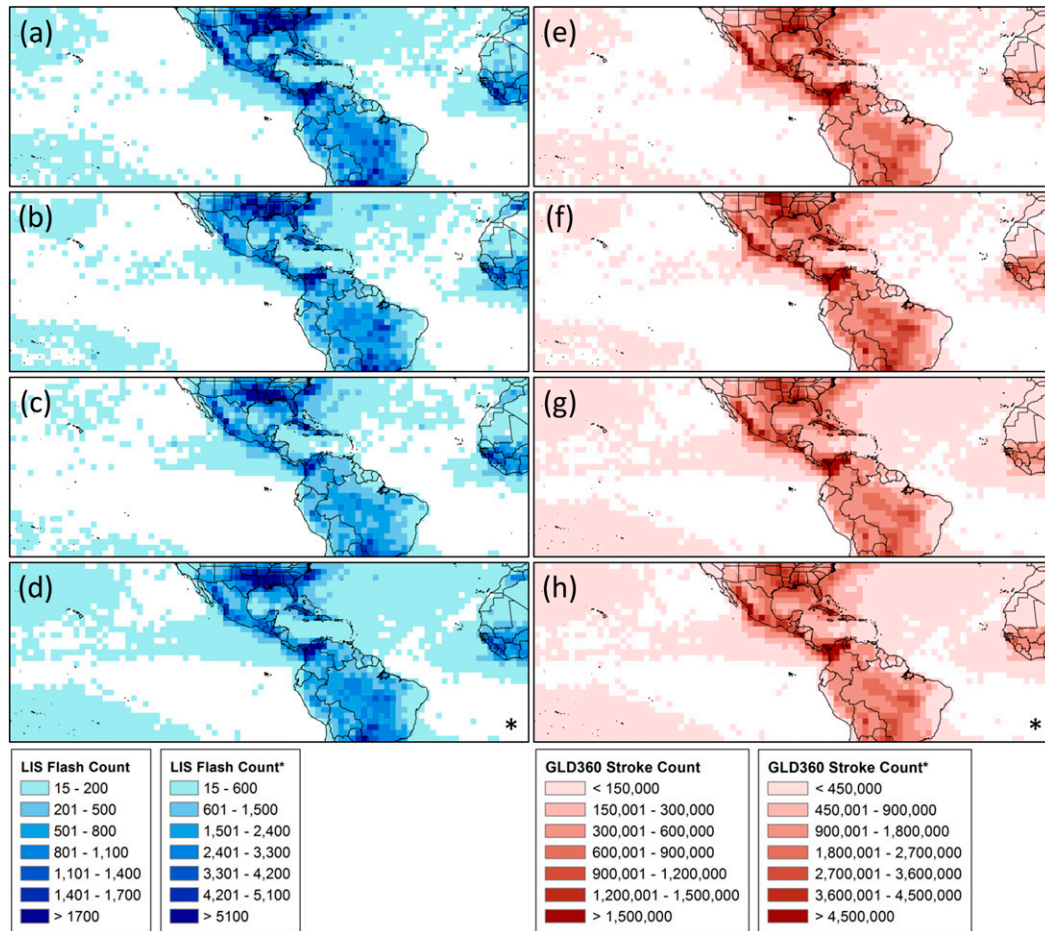
FIG. 1. Lightning Imaging Sensor flash counts during (a) 2012, (b) 2013, (c) 2014, and (d) 2012–14, along with the GLD360 stroke counts during (e) 2012, (f) 2013, (g) 2014, and (h) 2012–14. The color scale differs for (d) and (h), with colors representing 3 times the values depicted in (a)–(c) and (e)–(g). The limited LIS view time accounts for the much smaller LIS flash counts.

in magnitude. The GLD360 stroke counts are much larger because the network continuously monitors lightning activity rather than the individual swaths available from LIS. Despite the different sampling, the spatial lightning patterns depicted by the LIS and GLD360 are nearly identical, showing the adequacy of the LIS sampling. The LIS spatial distributions match higher-resolution climatologies (e.g., Albrecht et al. 2016), with maxima over the southeastern United States, Mexico, Cuba, Columbia, and Venezuela.

Table 1 provides counts for all LIS flashes, those matched using the operational GLD360 dataset, and those matched using the reprocessed GLD360 data during 2012–14. Table 1 also lists the relative DE for the operational and reprocessed data and the difference between these two values. A clear improvement between the operational and reprocessed data is evident

during each year in every region. The reprocessed data include ~70 000 additional matches per year in the study domain. The most pronounced differences between datasets occurred during 2014, with the relative DE improving by 23.3% and 20.8% over the United States and the oceans, respectively. Year-over-year improvement also is evident in each region. For example, from 2012 to 2013 to 2014, the relative DE in the Western Hemisphere (United States) improves from 38.7% (46.2%) to 43.5% (52.6%) to 51.4% (65.8%). The relative DE is greater over the oceans (52.6%) than over land (41.2%) during 2012–14.

Figures 2–5 further illustrate the spatial distributions of the pre- and postupgrade relative DE improvements. White grid boxes indicate where fewer than 15 LIS flashes were observed during the given period. The operational data during 2012 show the best relative DE over the Atlantic Ocean and Gulf of Mexico, with

TABLE 1. Counts for all LIS flashes within the study domain, those matched using the operational GLD360 dataset, and those matched using the reprocessed GLD360 data during 2012–14. GLD360 detection efficiency relative to TRMM LIS is listed for the operational and reprocessed data along with the difference between those two values.

	All LIS flashes	Operational matched	Reprocessed matched	Operational DE (%)	Reprocessed DE (%)	Difference (%)
2012						
Western Hemisphere	519 939	131 800	201 364	25.3	38.7	13.4
United States	92 518	31 112	42 756	33.6	46.2	12.6
All land	387 886	88 366	138 988	22.8	35.8	13.1
All oceans	132 053	43 434	62 736	32.9	47.5	14.6
2013						
Western Hemisphere	470 582	140 244	204 706	29.8	43.5	13.7
United States	85 188	30 866	44 818	36.2	52.6	16.4
All land	355 222	97 793	144 360	27.5	40.6	13.1
All oceans	115 360	42 451	60 346	36.8	52.3	15.5
2014						
Western Hemisphere	406 450	133 834	208 955	32.9	51.4	18.5
United States	77 223	32 812	50 843	42.5	65.8	23.3
All land	304 689	94 297	148 265	30.9	48.7	17.7
All oceans	101 761	39 537	60 690	38.9	59.6	20.8
2012–14						
Western Hemisphere	1 396 971	405 878	615 025	29.1	44.0	15.0
United States	254 929	94 790	138 417	37.2	54.3	17.1
All land	1 047 797	280 456	431 613	26.8	41.2	14.4
All oceans	349 174	125 422	183 772	35.9	52.6	16.7

poorer performance outside of those regions (Fig. 2a). The reprocessing results in much better performance throughout the study domain (Table 1; Fig. 2). During 2012, the reprocessed data show many more grid cells with relative DE greater than 40%, and the region with the best performance expands in every direction. Figure 2c confirms that the reprocessed data result in improvements throughout the study domain. The relative DE improves by >30% in many grid cells over the Pacific Ocean during 2012.

Figure 3 shows better performance during 2013 (vs 2012) and confirms the large improvements between the operational and reprocessed data. During 2013, the relative DE generally exceeds 60% in the western Atlantic and the Gulf of Mexico (Fig. 3b). Further relative DE improvement is evident during 2014 (Fig. 4) versus 2012 and 2013. The difference between the operational and reprocessed data is most apparent during 2014, with the relative DE improving by >10% in most grid cells (Fig. 4c). During 2014, the region with relative DE exceeding 60% includes the southern CONUS, the western Atlantic, the eastern Pacific, and the Gulf of Mexico (Fig. 4b). The performance in these regions also appears more spatially consistent than in the previous years.

The larger sample size in the 2012–14 composite provides the largest geographic coverage (i.e., more grid cells with at least 15 LIS flashes; Fig. 5). Although some

of the aforementioned variability mixes out in the composite, the improvement between the operational and reprocessed data is still very apparent. The reprocessed relative DE exceeds 40% throughout large portions of the study domain (Fig. 5b). Poorer performance appears over the southern Pacific and western Africa, but the relative DE still improves in these regions using the reprocessed data. The best 2012–14 relative DE appears over the western Atlantic, eastern Pacific, and the Gulf of Mexico.

In addition to the relative DE, the location accuracy also appears to have improved with the reprocessed data. Figure 6 illustrates the distance offsets between matched LIS flashes and GLD360 strokes for the operational and reprocessed GLD360 data. The distance offsets reported herein characterize imprecision in both the LIS and GLD360 observations, and thus should not be considered the absolute GLD360 location accuracy. Note that 44.3% of the matched LIS flashes contained two-plus GLD360 strokes (Table 2). In this case, the first GLD360 stroke (not the nearest in space or time) is considered the match. Figure 6 shows clear improvement in the location accuracy in the reprocessed GLD360 dataset. For the reprocessed data, there are more matches in the 0–13-km range (69.5% vs 60.1%) and fewer flashes with distance offsets greater than 13 km (Fig. 6). The mean (median) location difference decreased from 11.1 km (12.6 km) in the operational
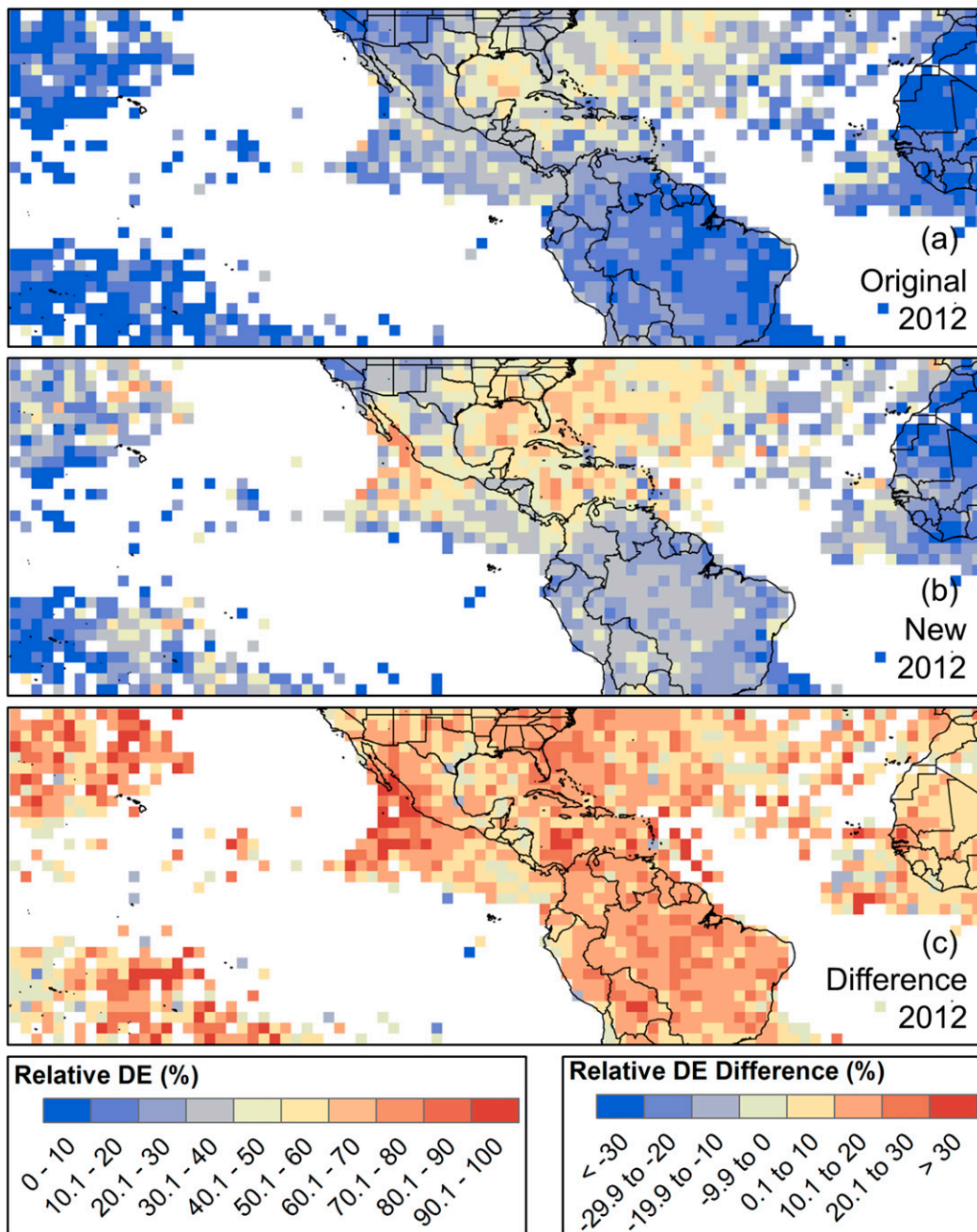
FIG. 2. Spatial distributions of the GLD360 detection efficiency relative to TRMM LIS flashes during 2012 using the (a) operational and (b) reprocessed data. The relative flash DE is computed by dividing the sum of the matched LIS flashes by the sum of all LIS flashes within $2° \times 2°$ grid cells. (c) Illustration of the difference between the relative DE for each grid cell (reprocessed minus operational). White areas in each panel indicate grid cells with fewer than 15 LIS flashes.

dataset to 9.5 km (10.9 km) in the reprocessed dataset. Using the nearest GLD360 stroke in space (rather than the first in time) results in mean (median) location differences of 8.7 km (7.0 km) for the reprocessed data.

The analysis now focuses on the results using the reprocessed data. The spatial plots (Figs. 2–5) are complemented by exploring the reprocessed GLD360 relative DE in individual regions (Table 3) and countries (Table 4). The best performance occurs over
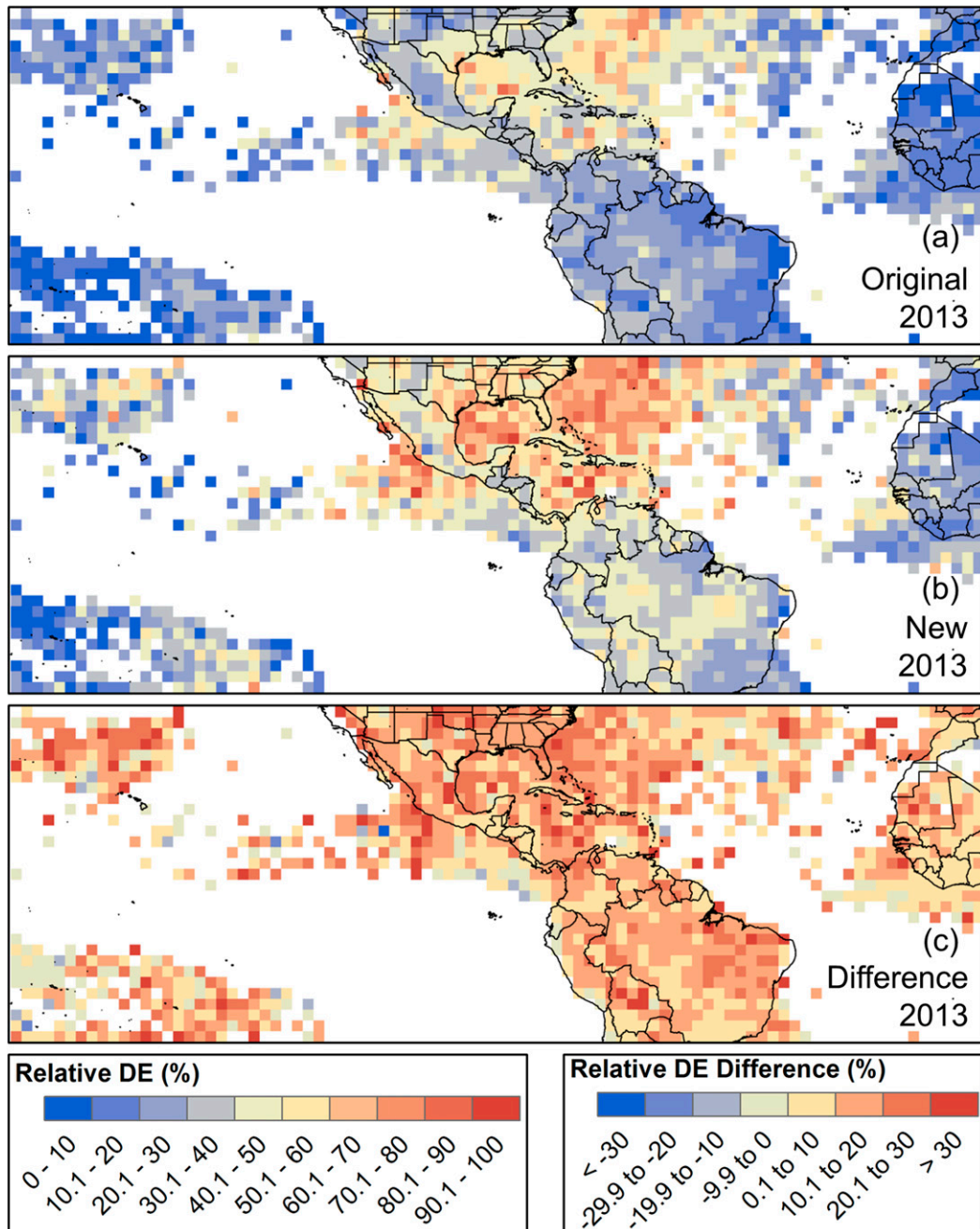
FIG. 3. As in Fig. 2, but for 2013.

North America with the poorest performance over western Africa. During 2012–14, the relative DE for the Caribbean Islands, Central America, and South America are 49.3%, 39.6%, and 37.4%, respectively. Year-over-year improvement is evident in each region, with relative DE increasing from 46.0% (17.5%) to 50.8% (23.5%) to 63.6% (26.2%) over North America (western Africa) during 2012, 2013, and 2014,

respectively. Table 4 lists the reprocessed relative DE for all countries in the study domain with more than 1000 LIS flashes during 2012–14. Although the performance is relatively uniform within each region, some variability exists. The best performance in North America, South America, Central America, the Caribbean Islands, and western Africa occurs in the United States (54.3%), Columbia (43.3%), Panama
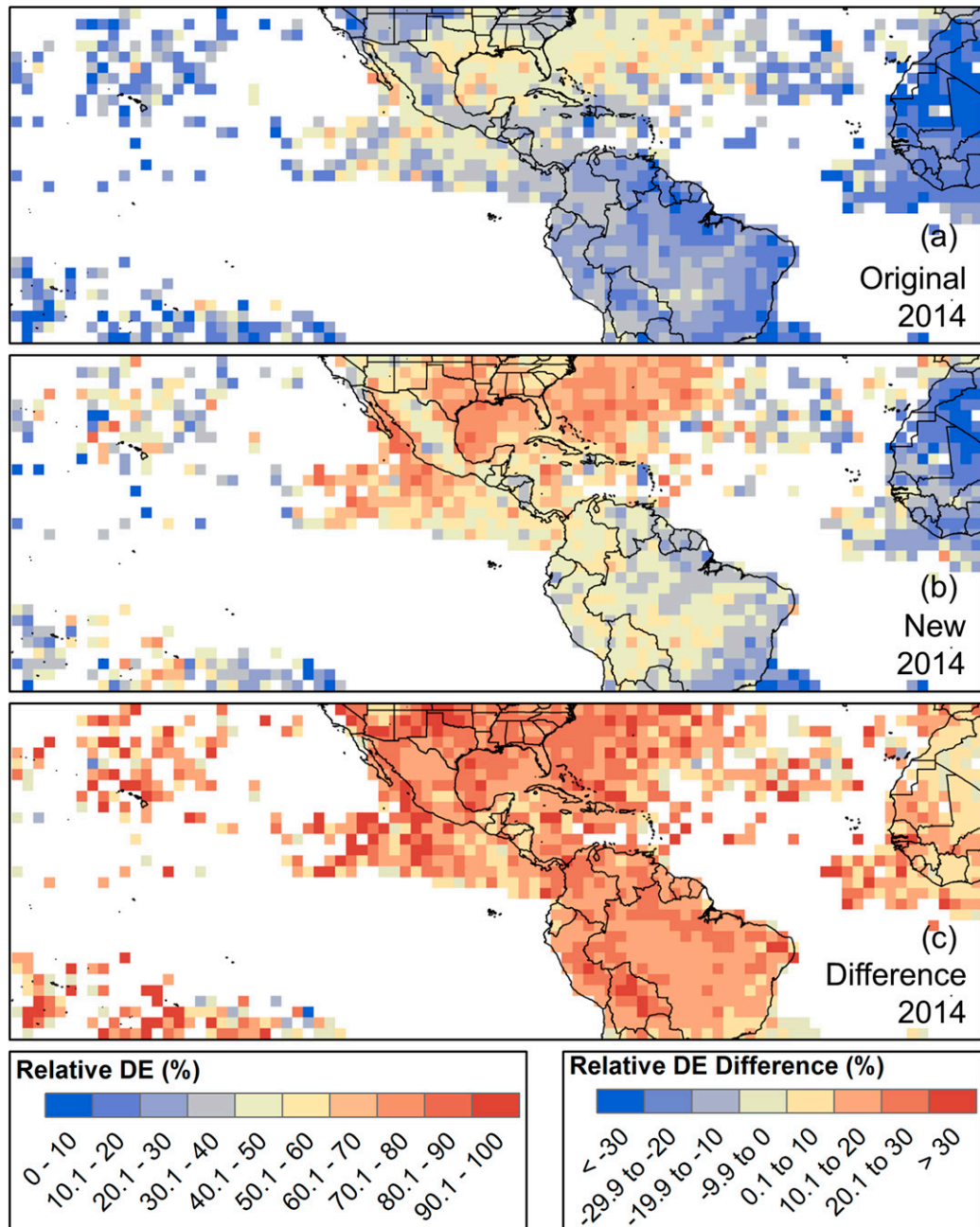
FIG. 4. As in Fig. 2, but for 2014.

(43.2%), Cuba (51.9%), and Guinea-Bissau (43.0%), respectively.

The analysis now shifts to discuss the characteristics of the LIS and GLD360 matches. Table 5 reveals that the matched LIS flashes have more groups (14.5) and events (70.6), last longer (18.6 ms), and are larger (379.3 km^2) than the unmatched LIS flashes (10.0, 41.3, 6.1 ms; 251.0 km^2, respectively). This finding is consistent with

previous intercomparisons of LIS data with data from WWLLN (Rudlosky and Shea 2013) and ENTLN (Rudlosky 2015). Koshak (2010) introduced the maximum number of events per group (MNEG) and the maximum group area (MGA) as potential return stroke identifiers, and those metrics are also greater for the matched LIS flashes (13.4, 331.6 km^2, respectively) than the unmatched LIS flashes (8.9, 221.5 km^2, respectively).
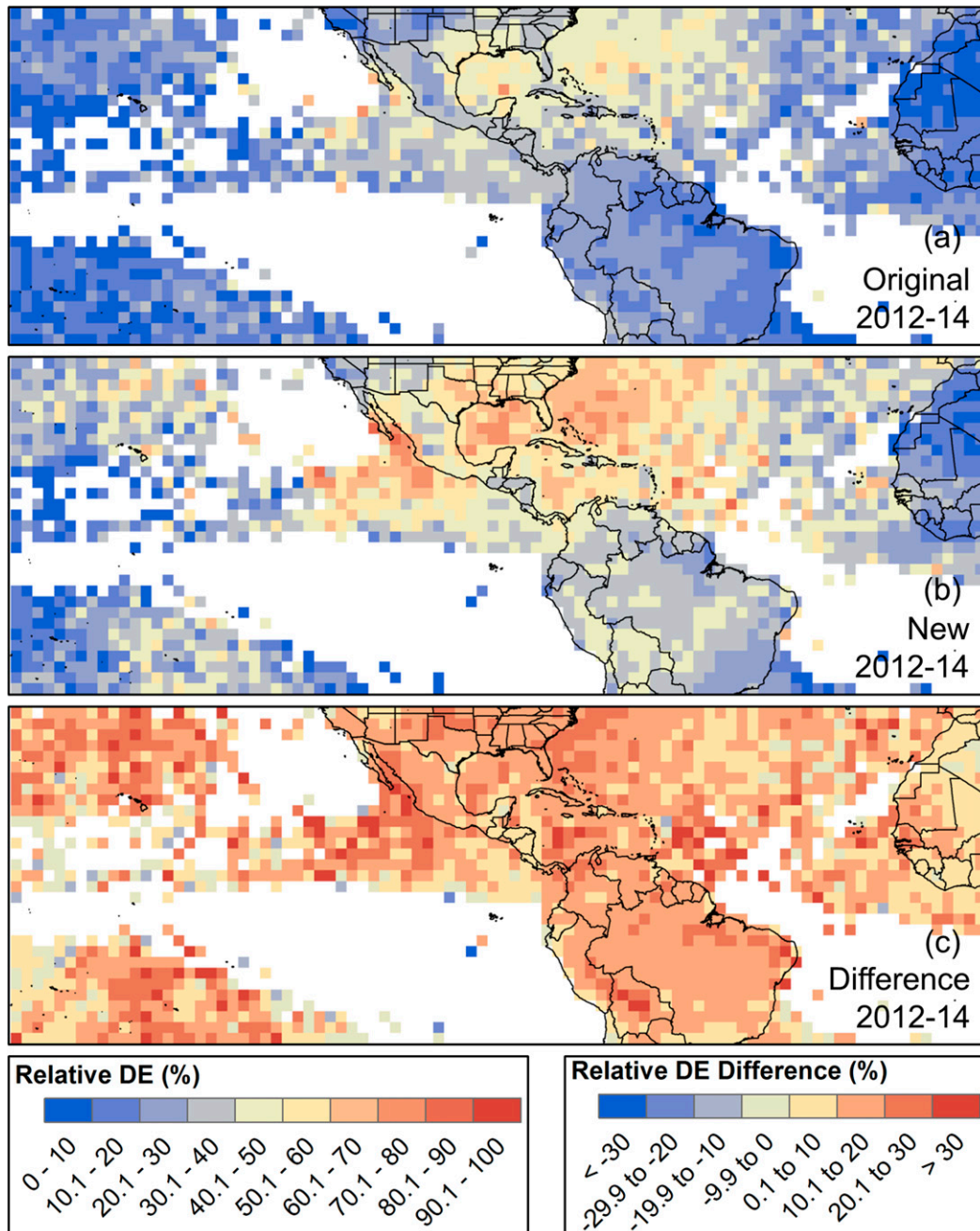
FIG. 5. As in Fig. 2, but for the 3-yr composite, 2012–14.

This suggests that many of the matched LIS flashes are CG (i.e., containing return strokes), while many of the unmatched flashes may be IC.

Table 5 shows that the relative DE depends on the LIS characteristics, and Fig. 7 provides further confirmation. The relative DE is 36.2% for LIS flashes shorter than 45 ms, 64.7% for flashes lasting between 495 and 540 ms, and 81.3% for flashes longer than 1755 ms (Fig. 7a). The relative DE is ~80% for all LIS flashes lasting longer than 1 s (1000 ms). Thus, the longer the LIS flash, the more likely the GLD360 is to observe it. Figures 7b–d show rapid increases in the relative DE as each of the LIS characteristics increases before settling at ~70% for greater values. The relative DE is 29.3% (34.8%) for LIS flashes with MNEG (group count) less than 4, 69.2% (64.7%) for LIS flashes with MNEG (group
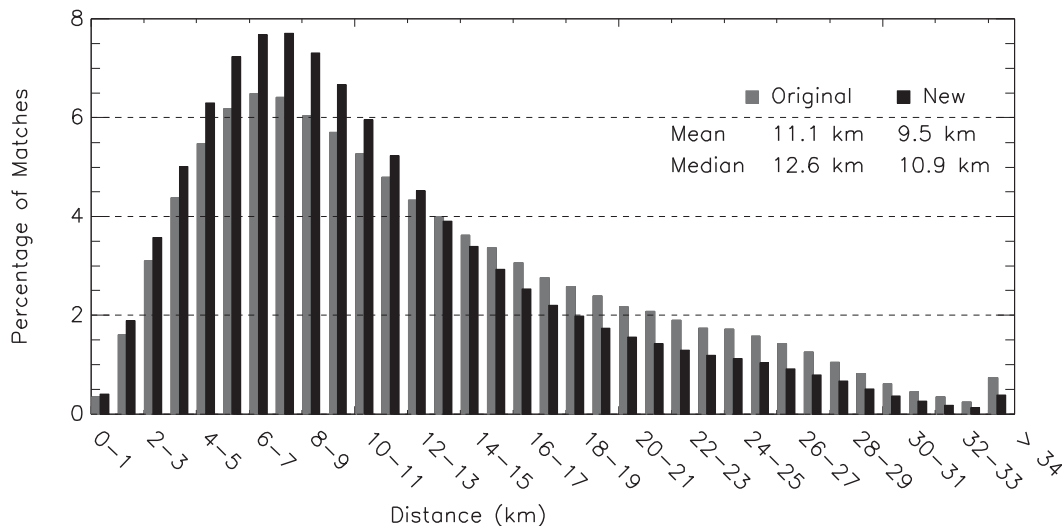
FIG. 6. Distance offset between matched LIS flashes and GLD360 strokes for the operational (original, gray) and reprocessed (new, black) data. For the case of multiple GLD360 strokes related to one LIS flash, the first GLD360 stroke in time (not the nearest in space or time) is considered the match for this plot.

count) between 48 and 52, and 70.0% (65.1%) for LIS flashes with MNEG (group count) greater than 156. Figure 7c reveals that the distributions of relative DE based on flash area and MGA are remarkably similar. The relative DE is 28.7% (26.5%) for LIS flashes with MGA (flash area) less than $100 \, \text{km}^2$, 69.4% (68.7%) for LIS flashes with MGA (flash area) between 1100 and $1200 \, \text{km}^2$, and 72.2% (73.0%) for LIS flashes with MGA (flash area) greater than $3900 \, \text{km}^2$. The relative DE is 33.3% for LIS flashes with fewer than 20 events, 67.3% for LIS flashes with between 300 and 320 events, and 68.2% for LIS flashes with more than 780 events (Fig. 7d). For each LIS characteristic examined, the greater the value, the more likely the GLD360 is to observe the LIS flash.

Most of the matched LIS flashes have only one related GLD360 stroke (55.7%), but 44.3% (13.9%) of the matched LIS flashes contain two-plus (four plus) related GLD360 strokes (Table 2). Figure 8a illustrates the distribution of first-stroke estimated peak current (I_p) by the total number of GLD360 strokes associated with each matched LIS flash. Single-stroke flashes are more likely to have weaker I_p (i.e., -15 to $+15 \, \text{kA}$) than multistroke flashes. Alternatively, as the number of strokes increases, so does the likelihood that the magnitude of the first-stroke I_p exceeds $-50 \, \text{kA}$ ($+50 \, \text{kA}$). Table 6 reveals that all of the LIS characteristics increase with increasing stroke count. Single-stroke flashes have the fewest average number of groups (12.0) and events (55.7) and are both shorter (8.4 ms) and smaller ($337.8 \, \text{km}^2$) than the multistroke flashes.

LIS flashes with four-plus related GLD360 strokes have the most groups (20.4) and events (110.6) and are the longest (61.1 ms) and largest ($492.7 \, \text{km}^2$) LIS flashes.

For LIS flashes with multiple GLD360 strokes, 57.3% contain subsequent strokes with greater I_p than the initial stroke I_p (not shown). Stronger subsequent strokes occur in 48.9%, 61.8%, and 68.2% of matched LIS flashes with two, three, and four-plus related GLD360 strokes, respectively (not shown). Figure 8b displays the fraction of GLD360 LIS matches with stronger subsequent strokes based on the first-stroke I_p and total stroke count. The vast majority of multistroke flashes with I_p in the -10 to $+10 \, \text{kA}$ range have stronger

TABLE 2. Distribution of GLD360 strokes that occur during matched LIS flashes. All matches have at least one associated stroke, 44.3% have two or more related strokes, and 13.9% have four or more related strokes.

Stroke count	Occurrences (count)	Frequency of occurrence (%)
1+	615 025	100.0
2+	272 427	44.3
3+	147 608	24.0
4+	85 271	13.9
5+	51 197	8.3
6+	31 466	5.1
7+	19 666	3.2
8+	12 504	2.0
9+	8076	1.3
10+	5245	0.9

TABLE 3. Count of all LIS flashes, matched LIS flashes, and the relative DE over the landmasses of North America, South America, Central America, the Caribbean Islands, and western Africa using the reprocessed GLD360 data during 2012–14.

	All LIS flashes	Matched LIS flashes	Relative DE (%)
2012			
North America	131 825	60 666	46.0
South America	195 909	63 943	32.6
Central America	10 579	4131	39.0
Caribbean Islands	5575	2549	45.7
Western Africa	43 858	7664	17.5
2013			
North America	116 349	59 104	50.8
South America	181 933	69 075	38.0
Central America	8675	3199	36.9
Caribbean Islands	7010	3265	46.6
Western Africa	41 122	9672	23.5
2014			
North America	108 490	69 014	63.6
South America	145 058	62 653	43.2
Central America	6239	2758	44.2
Caribbean Islands	7232	3963	54.8
Western Africa	37 540	9823	26.2
2012–14			
North America	356 664	188 784	52.9
South America	522 900	195 671	37.4
Central America	25 493	10 088	39.6
Caribbean Islands	19 817	9777	49.3
Western Africa	122 520	27 159	22.2

TABLE 4. Count of all LIS flashes, matched LIS flashes, and the relative DE over the landmasses of all countries in the study domain with at least 1000 LIS flashes using the reprocessed GLD360 data during 2012–14.

Region	Country	All LIS flashes	Matched LIS flashes	Relative DE (%)
All	All Land	104 7797	431 613	41.2
North America	United States	254 741	138 350	54.3
	Mexico	101 923	50 434	49.5
South America	Argentina	8868	3419	38.6
	Bolivia	37 215	15 497	41.6
	Brazil	312 194	110 563	35.4
	Colombia	63 307	27 407	43.3
	Guyana	3343	1044	31.2
	Paraguay	25 143	9270	36.9
	Peru	32 608	12 994	39.8
	Suriname	2115	689	32.6
	Venezuela	31 031	12 232	39.4
	Ecuador	5009	1797	35.9
Central America	Costa Rica	2471	926	37.5
	El Salvador	1952	712	36.5
	Guatemala	7325	3036	41.4
	Honduras	4757	1749	36.8
	Nicaragua	4606	1770	38.4
	Panama	4382	1895	43.2
Caribbean Islands	Cuba	13 362	6933	51.9
	Dominican Republic	2005	911	45.4
	Haiti	2525	1024	40.6
Western Africa	Algeria	4103	417	10.2
	Burkina Faso	9794	2340	23.9
	Ghana	11 265	2468	21.9
	Guinea	17 755	4924	27.7
	Guinea-Bissau	2140	921	43.0
	Ivory Coast	15 260	2800	18.3
	Liberia	6533	844	12.9
	Mali	24 073	5963	24.8
	Mauritania	9265	1960	21.2
	Morocco	10 415	1380	13.3
	Senegal	4962	1768	35.6
	Sierra Leone	5713	1098	19.2

subsequent strokes. This value is most pronounced for flashes with three and four-plus GLD360 strokes, with greater than 95% containing stronger subsequent strokes. The likelihood of stronger subsequent strokes increases with stroke count for all I_p values. This finding suggests that the GLD360 sometimes observes the initial cloud pulses associated with flashes that eventually strike ground.

4. Discussion

The recent GLD360 upgrade motivated analysis of the operational GLD360 dataset alongside data that have been reprocessed using the upgraded algorithms. There is a clear increase in the fraction of LIS flashes detected by the GLD360 between the operational and reprocessed data. The relative DE improvement appears during each year in every region, and year-over-year improvement also is evident in each region for both datasets. The reprocessed relative DE increases from 46.0% (2012) to 50.8% (2013) to 63.6% (2014) over North America. Algorithm changes alone cannot explain the improvement from

year to year, but this observation is consistent with the improved performance of other ground-based lightning detection networks over time. Ground-based lightning data are provided by private vendors, who continually work to improve their networks by adding sensors, relocating sensors, improving hardware, and upgrading software. Consistent improvement between the operational and reprocessed datasets in all of the studied domains shows that the major GLD360 performance improvement is related to the algorithm upgrades and not hardware changes (e.g., the addition of sensors).

Broad geographic areas have relatively uniform GLD360 performance, but regional and interregional performance variability also exists. The best performance

TABLE 5. Average characteristics (and standard errors) of all LIS flashes, those observed by the GLD360 (matched), and those not observed by the GLD360 using the reprocessed GLD360 data during 2012–14.

2012–14	All LIS	Matched	Unmatched
Groups (count)	11.9 ± 0.01	14.5 ± 0.02	10.0 ± 0.01
Events (count)	54.1 ± 0.07	70.6 ± 0.13	41.3 ± 0.08
Duration (ms)	11.6 ± 0.30	18.6 ± 0.51	6.1 ± 0.35
Area (km^2)	307.0 ± 0.28	379.3 ± 0.50	251.0 ± 0.30
MNEG (count)	10.9 ± 0.01	13.4 ± 0.02	8.9 ± 0.01
MGA (km^2)	269.6 ± 0.26	331.6 ± 0.46	221.5 ± 0.27

in North America, South America, Central America, the Caribbean Islands, and western Africa occurs in the United States (54.3%), Columbia (43.3%), Panama (43.2%), Cuba (51.9%), and Guinea-Bissau (43.0%), respectively. The reprocessed relative DE exceeds 40% throughout large portions of the study domain. During 2014, the region with relative DE exceeding 60% includes southern CONUS, the western Atlantic, the eastern Pacific, and the Gulf of Mexico. As previously shown for other VLF networks (e.g., Biswas and Hobbs 1990; Orville and Huffines 2001; Rudlosky and Fuelberg 2010; Orville et al. 2011; Said et al. 2013; Hutchins et al. 2013; Rudlosky and Shea 2013), the GLD360 relative DE is greater over the oceans

(52.6%) than over land (41.2%). The GLD360 detects more than 60% of the LIS flashes over the National Hurricane Center Atlantic marine forecast areas, which supports use of the GLD360 for investigations of oceanic storms, especially tropical storms and hurricanes in the Atlantic basin.

Direct flash-to-stroke comparisons provide several important insights into the relationship between the ground- and satellite-based lightning observations. The GLD360 relative DE strongly depends on the LIS characteristics. The matched LIS flashes have more groups (14.5) and events (70.6), last longer (18.6 ms), and are larger (379.3 km^2) than the unmatched LIS flashes (10.0, 41.3, 6.1 ms, 251.0 km^2, respectively). For each LIS characteristic examined, the greater the value, the more likely the GLD360 is to observe the LIS flash. The LIS characteristics also increase with increasing GLD360 stroke count. Single-stroke flashes have the fewest LIS groups and events and are both shorter and smaller than the multistroke flashes. LIS flashes with four-plus related GLD360 strokes have the most groups and events and are the longest and largest LIS flashes. These findings show that lightning intensity is observable by both ground- and space-based lightning observation networks, albeit with different measures of intensity. While most present lightning-derived forecasting tools display the occurrence and frequency
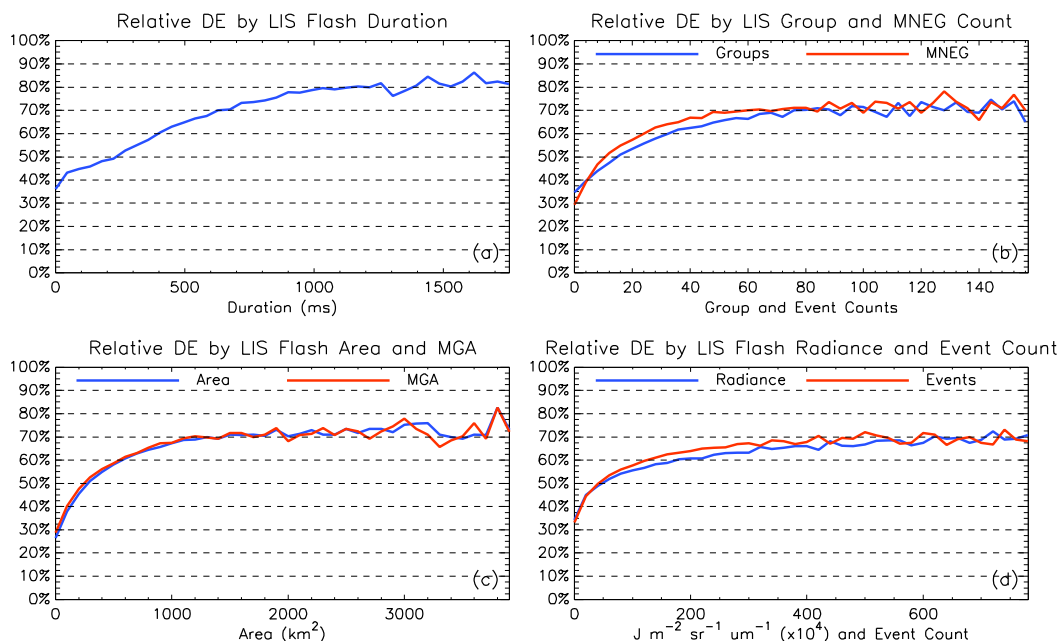
FIG. 7. Histograms of the GLD360 DE relative to TRMM LIS flashes based on the LIS reported flash characteristics, including (a) flash duration, (b) number of groups and maximum number of events per group, (c) flash area and maximum group area, and (d) number of events and flash radiance.
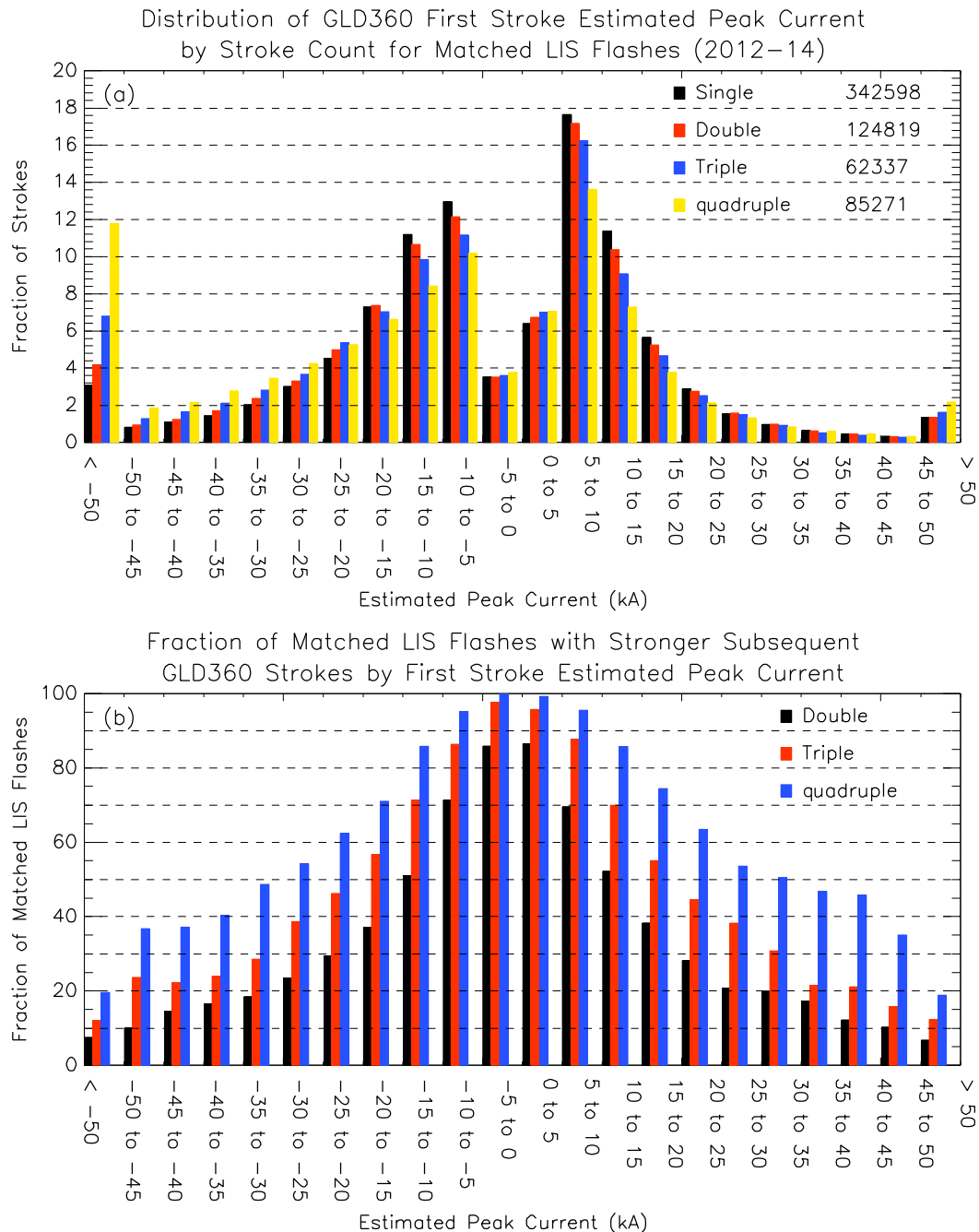
Distribution of GLD360 First Stroke Estimated Peak Current
by Stroke Count for Matched LIS Flashes (2012–14)

Fraction of Matched LIS Flashes with Stronger Subsequent
GLD360 Strokes by First Stroke Estimated Peak Current

FIG. 8. (a) Distribution of first-stroke estimated peak current (i.e., I_p) by the number of GLD360 strokes associated with each matched LIS flash. (b) Fraction of matched LIS flashes with stronger subsequent strokes categorized by first-stroke I_p and total stroke count.

of lightning flashes, many additional lightning intensity metrics are descriptive of storm strength and morphology (e.g., Peterson and Liu 2013; Peterson et al. 2016).

Most of the matched LIS flashes have only one related GLD360 stroke (55.7%), but 44.3% (13.9%) of the matches contain two-plus (four plus) related GLD360 strokes. For LIS flashes with multiple GLD360 strokes, 57.3% contain subsequent strokes with greater I_p than the initial stroke I_p. Stronger subsequent strokes occur in 48.9%, 61.8%, and 68.2% of matched LIS flashes with two, three, and four-plus related GLD360 strokes,

TABLE 6. Average characteristics (and standard errors) of LIS flashes observed by the GLD360 that contain only one related GLD360 stroke (single), those with two related strokes (double), those with three related strokes (triple), and those with four or more related strokes (quadruple+). This table characterizes the reprocessed GLD360 data during 2012–14.

2012–14	Single	Double	Triple	Quadruple+
Groups (count)	12.0 ± 0.01	15.7 ± 0.01	17.6 ± 0.01	20.4 ± 0.01
Events (count)	55.7 ± 0.08	75.1 ± 0.06	88.6 ± 0.05	110.6 ± 0.07
Duration (ms)	8.4 ± 0.33	14.9 ± 0.23	24.1 ± 0.18	61.1 ± 0.25
Area (km^2)	337.8 ± 0.35	390.2 ± 0.22	430.3 ± 0.16	492.7 ± 0.21
MNEG (count)	12.1 ± 0.01	13.7 ± 0.01	15.1 ± 0.01	16.9 ± 0.01
MGA (km^2)	300.2 ± 0.33	339.5 ± 0.21	371.1 ± 0.15	417.3 ± 0.19

respectively. Zhu et al. (2015) showed that the mean first to subsequent stroke field peak ratio is 2.4 over Florida, and that 34% of multistroke flashes have at least one subsequent stroke whose field peak is greater than that of the first stroke. Poelman et al. (2013) found that the first stroke has a greater chance of being detected than the subsequent strokes because first strokes exhibited greater peak currents than the subsequent strokes in 57 negative CG flashes in Belgium. Strong initial strokes are even more likely over the oceans than over land. Cooray et al. (2014) suggested that higher cloud potentials are required to initiate ground flashes in maritime storms, and that lightning flashes initiated under higher potentials harbor larger first return stroke currents. The vast majority of multistroke flashes with first-stroke I_p between -10 and $+10$ kA contain stronger subsequent strokes. This suggests that the GLD360 sometimes observes the initial cloud pulses associated with flashes that eventually strike ground. Since the GLD360 does not differentiate between IC and CG strokes, additional research will be required to confirm this observation.

Analysis of the distance offsets between matched LIS flashes and GLD360 strokes reveals clear improvement in location accuracy in the reprocessed dataset. The mean (median) location difference improved from 11.1 km (12.6 km) in the operational dataset to 9.5 km (10.9 km) in the reprocessed dataset. For multistroke flashes, using the nearest GLD360 stroke in space (rather than the first in time) results in mean (median) location differences of 8.7 km (7.0 km) for the reprocessed data. The similarity between the flash and stroke locations reported by the optical and radio systems is encouraging for GLM applications. The close proximity suggests that the GLD360 data can help validate the GLM, and future forecasting tools could benefit from the combination of ground- and space-based lightning observations.

REFERENCES

Albrecht, R., S. Goodman, D. Buechler, R. Blakeslee, and H. Christian, 2016: Where are the lightning hotspots on Earth? *Bull. Amer. Meteor. Soc.*, **97**, 2051–2068, doi:10.1175/BAMS-D-14-00193.1.

Biswas, K. R., and P. V. Hobbs, 1990: Lightning over the Gulf Stream. *Geophys. Res. Lett.*, **17**, 941–943, doi:10.1029/GL017i007p00941.

Bitzer, P., J. Burchfield, and H. Christian, 2016: A Bayesian approach to assess the performance of lightning detection systems. *J. Atmos. Oceanic Technol.*, **33**, 563–578, doi:10.1175/JTECH-D-15-0032.1.

Boccippio, D. J., W. J. Koshak, and R. J. Blakeslee, 2002: Performance assessment of the optical transient detector and Lightning Imaging Sensor. Part I: Predicted diurnal variability. *J. Atmos. Oceanic Technol.*, **19**, 1318–1332, doi:10.1175/1520-0426(2002)019<1318:PAOTOT>2.0.CO;2.

Cecil, D. J., D. E. Buechler, and R. J. Blakeslee, 2014: Gridded lightning climatology from TRMM-LIS and OTD: Dataset description. *Atmos. Res.*, **135–136**, 404–414, doi:10.1016/j.atmosres.2012.06.028.

Christian, H. J., R. J. Blakeslee, and S. J. Goodman, 1992: Lightning Imaging Sensor (LIS) for the Earth Observing System. NASA Tech. Memo. NASA TM-4350, 44 pp. [Available from Center for Aerospace Information, P.O. Box 8757, Baltimore–Washington International Airport, Baltimore, MD 21240.]

——, and Coauthors, 1999: The Lightning Imaging Sensor. *11th International Conference on Atmospheric Electricity*, H. J. Christian, Ed., NASA Conf. Publ. NASA/CP-1999-209261, 746–749.

——, and Coauthors, 2003: Global frequency and distribution of lightning as observed from space by the optical transient detector. *J. Geophys. Res.*, **108**, 4005, doi:10.1029/2002JD002347.

Cooray, V., R. Jayaratne, and K. L. Cummins, 2014: On the peak amplitude of lightning return stroke currents striking the sea. *Atmos. Res.*, **149**, 372–376, doi:10.1016/j.atmosres.2013.07.012.

Goodman, S. J., and Coauthors, 2013: The GOES-R Geostationary Lightning Mapper (GLM). *Atmos. Res.*, **125–126**, 34–49, doi:10.1016/j.atmosres.2013.01.006.

Hutchins, M. L., R. H. Holzworth, K. S. Virts, J. M. Wallace, and S. Heckman, 2013: Radiated VLF energy differences of land and oceanic lightning. *Geophys. Res. Lett.*, **40**, 2390–2394, doi:10.1002/grl.50406.

Koshak, W. J., 2010: Optical characteristics of OTD flashes and the implications for flash-type discrimination. *J. Atmos. Oceanic Technol.*, **27**, 1822–1838, doi:10.1175/2010JTECHA1405.1.

Liu, C., and S. Heckman, 2012: Total lightning data and real-time severe storm prediction. *TECO-2012: WMO Tech. Conf. on Meteorological and Environmental Instruments and Methods of Observation*, Brussels, Belgium, World Meteorological Organization, P5(10). [Available online at http://www.wmo.int/pages/prog/www/IMOP/publications/IOM-109_TECO-2012/Session5/P5_10_Liu_Total_Lightning_Data_and_Real-Time_Severe_Storm_Prediction.pdf.]

Mach, D. M., H. J. Christian, R. J. Blakeslee, D. J. Boccipio, S. J. Goodman, and W. L. Boeck, 2007: Performance assessment of the optical transient detector and Lightning Imaging Sensor. *J. Geophys. Res.*, **112**, D09210, doi:10.1029/2006JD007787.

Mallick, S., and Coauthors, 2014: Evaluation of the GLD360 performance characteristics using rocket-and-wire triggered lightning data. *Geophys. Res. Lett.*, **41**, 3636–3642, doi:10.1002/2014GL059920.

Orville, R. E., and G. R. Huffines, 2001: Cloud-to-ground lightning in the United States: NLDN results in the first decade, 1989–98. *Mon. Wea. Rev.*, **129**, 1179–1193, doi:10.1175/1520-0493(2001)129<1179:CTGLIT>2.0.CO;2.

——, ——, W. R. Burrows, and K. L. Cummins, 2011: The North American Lightning Detection Network (NALDN)—Analysis of flash data: 2001–09. *Mon. Wea. Rev.*, **139**, 1305–1322, doi:10.1175/2010MWR3452.1.

Peterson, M. J., and C. Liu, 2013: Characteristics of lightning flashes with exceptional illuminated areas, durations, and optical powers and surrounding storm properties in the tropics and inner subtropics. *J. Geophys. Res. Atmos.*, **118**, 11 727–11 740, doi:10.1002/jgrd.50715.

——, W. Deierling, C. Liu, D. Mach, and C. Kalb, 2016: The properties of optical lightning flashes and the clouds they illuminate. *J. Geophys. Res. Atmos.*, **122**, 423–442, doi:10.1002/2016JD025312.

Poelman, D., W. Schulz, and C. Vergeiner, 2013: Performance characteristics of distinct lightning detection networks covering Belgium. *J. Atmos. Oceanic Technol.*, **30**, 942–951, doi:10.1175/JTECH-D-12-00162.1.

Pohjola, H., and A. Mäkelä, 2013: The comparison of GLD360 and EUCLID lightning location systems in Europe. *Atmos. Res.*, **123**, 117–128, doi:10.1016/j.atmosres.2012.10.019.

Rodger, C. J., J. B. Brundell, R. L. Dowden, and N. R. Thomson, 2004: Location accuracy of long distance VLF lightning location network. *Ann. Geophys.*, **22**, 747–758, doi:10.5194/angeo-22-747-2004.

Rudlosky, S. D., 2015: Evaluating ENTLN performance relative to TRMM/LIS. *J. Oper. Meteor.*, **3**, 11–20, doi:10.15191/nwajom.2015.0302.

——, and H. E. Fuelberg, 2010: Pre- and postupgrade distributions of NLDN reported cloud-to-ground lightning characteristics in the contiguous United States. *Mon. Wea. Rev.*, **138**, 3623–3633, doi:10.1175/2010MWR3283.1.

——, and D. T. Shea, 2013: Evaluating WWLLN performance relative to TRMM/LIS. *Geophys. Res. Lett.*, **40**, 2344–2348, doi:10.1002/grl.50428.

Said, R. K., and M. Murphy, 2016: GLD360 upgrade: Performance analysis and applications. *Extended Abstracts, 24th Int. Lightning Detection Conf. and Sixth Int. Lightning Meteorology Conf.*, San Diego, CA, Vaisala, 8 pp. [Available online at http://www.vaisala.com/en/events/ildcilmc/archive/Pages/ILDCILMC-2016-Archive.aspx.]

——, U. S. Inan, and K. L. Cummins, 2010: Long-range lightning geolocation using a VLF radio atmospheric waveform bank. *J. Geophys. Res.*, **115**, D23108, doi:10.1029/2010JD013863.

——, M. B. Cohen, and U. S. Inan, 2013: Highly intense lightning over the oceans: Estimated peak currents from global GLD360 observations. *J. Geophys. Res. Atmos.*, **118**, 6905–6915, doi:10.1002/jgrd.50508.

Simpson, J., R. F. Adler, and G. R. North, 1988: A proposed Tropical Rainfall Measuring Mission (TRMM) satellite. *Bull. Amer. Meteor. Soc.*, **69**, 278–295, doi:10.1175/1520-0477(1988)069<0278:APTRMM>2.0.CO;2.

Thomas, R. J., and Coauthors, 2000: Comparison of ground-based 3-dimensional lightning mapping observations with satellite-based LIS observations in Oklahoma. *Geophys. Res. Lett.*, **27**, 1703–1706, doi:10.1029/1999GL010845.

Ushio, T., S. Heckman, K. Driscoll, D. Boccippio, H. Christian, and Z. I. Kawasaki, 2002: Cross-sensor comparison of the Lightning Imaging Sensor (LIS). *Int. J. Remote Sens.*, **23**, 2703–2712, doi:10.1080/01431160110107789.

Zhang, D., K. L. Cummins, A. Nag, M. Murphy, and P. Bitzer, 2016: Evaluation of the National Lightning Detection Network upgrade using the Lightning Imaging Sensor. *Extended Abstracts, 24th Int. Lightning Detection Conf. and Sixth Int. Lightning Meteorology Conf.*, San Diego, CA, Vaisala, 10 pp. [Available online at http://www.vaisala.com/en/events/ildcilmc/archive/Pages/ILDCILMC-2016-Archive.aspx.]

Zhu, Y., V. A. Rakov, S. Mallick, and M. D. Tran, 2015: Characterization of negative cloud-to-ground lightning in Florida. *J. Atmos. Sol.-Terr. Phys.*, **136A**, 8–15, doi:10.1016/j.jastp.2015.08.006.